

Effects of Electron Correlation on the Transport through a Quantum Dot Superlattice

Yoshihide TANAKA* and Akira OGURI

Department of Material Science, Osaka City University, Sumiyoshi-ku, Osaka 558-8585, Japan

(Received March 14, 2003)

We study correlation effects on the transport through a quantum dot superlattice using a two-dimensional Hubbard model connected to two noninteracting leads. To calculate the zero-temperature conductance away from half-filling, we have used the non-magnetic solution of the Hartree-Fock approximation for the unperturbed Green's function, and then take into account the electron correlation beyond the mean field theory through the second-order self-energy corrections with respect to the residual interaction. When the value of the onsite potential ϵ_d or the repulsion U is changed, the conductance shows a number of peaks corresponding to the resonance states passing through the Fermi energy. The behavior of the resonance states for correlated electrons can be investigated using the eigenvalue of the effective Hamiltonian for a quasi-particle of a local Fermi liquid. We calculate the eigenvalue using the second-order self-energy, and show explicitly that it can be compared with the conductance peak.

KEYWORDS: conductance, electron correlation, Hubbard model, two-dimension, perturbation expansion, electron-hole asymmetry

1. Introduction

Systems of nanometer scale and artificial structures, such as quantum dots and quantum wires, have been a subject of current interest. In these systems the Coulomb interaction seems to play an important role on the transport properties. For instance, the Kondo effect in quantum dots has been studied intensively¹⁻⁵⁾ and the experiments have been shown to be in qualitative agreement with theoretical predictions.^{6,7)} The artificial molecule which can be realized by arranging two or more quantum dots is another example.^{8,9)} Also, an interesting quantum dot superlattice showing the ferromagnetism or d -wave superconductivity has been designed theoretically.^{10,11)} The proposed superlattice consists of a two-dimensional network of quantum wires, and is described by a Hubbard model that is derived based on the local density approximation.

In theoretical studies of the transport properties of strongly correlated electrons, accurate numerical approaches such as the numerical renormalization group^{12,13)} and quantum Monte Carlo methods^{14,15)} have been used successfully. However, the analytic methods, which are complementary to the numerical ones, are also required to clarify the underlying physics comprehensively. The perturbation theory in the Coulomb interaction is one of such approaches. For instance in the Kondo problem,¹⁶⁾ the perturbation expansion with respect to U has shown to work quite

* E-mail tanakay@sci.osaka-cu.ac.jp

well to describe the low-energy Fermi-liquid behavior.^{17,18)} The perturbation theory can also describe properly the low-voltage behavior of the out-of-equilibrium Kondo system under finite bias voltages.^{5,19)} Furthermore, based on the analytic properties of the vertex function, the transport equation for the Fermi liquid derived by Éliashberg²⁰⁾ has been shown to have a link to the Landauer formula for the conductance of the correlated electrons.²¹⁾

We have been studying the transport properties of a quantum dot superlattice based on a Hubbard model coupled to two noninteracting leads.²²⁾ A schematic picture of the model is illustrated in Fig. 1: the system consists of a Hubbard model of $N_C (= N \times M)$ sites and two semi-infinite noninteracting leads of M channels at left and right, where N and M are the size in the x - and y -direction, respectively. We have considered the square lattice for simplicity. At this moment this model itself might have no direct correspondence to experiments. Nevertheless, it seems to contain essential features of two-dimensional network of quantum dots or atomic systems, and we believe that it could be realized some day in near future. In this kind of the system that coupled to the noninteracting leads, the contribution of the vertex corrections on the conductance vanishes at zero temperature.²³⁾ Thus, at $T = 0$, the conductance can be written in terms of the single-particle Green's function at the Fermi energy $\omega = 0$. In previous work we have calculated the conductance at half-filling, where the average number of the electron per site is one, using the order U^2 self-energy. The conductance shows some peaks as a function of U when the hopping matrix elements are anisotropic. We found at half-filling that the position of the resonance peaks can be analyzed through the eigenvalues of the effective Hamiltonian for free quasi-particles. However, in actual quantum dots the half-filled situation is expected only for a special value of the gate voltage, which can be related to the onsite energy ϵ_d of the theoretical model. Therefore, real systems are usually in away from half-filling, so that it should be examined on the same basis.

The purpose of this paper is to study the correlation effects on the transport properties away from half-filling. In this case, the average number of electrons per site is not unity, and the spatial distribution of the charge is not uniform. Therefore, as the density functional theory states,²⁴⁾ the charge distribution should be determined accurately to obtain the ground-state properties correctly. Note that the charge distribution is uniform at half-filling, so that we did not have to take any care over the details of the distribution in the previous study. In the present study, we have used a non-magnetic solution of the Hartree-Fock approximation to determine the unperturbed Green's function, and then take into account the correlation effects beyond the mean field approximation through the second-order self-energy corrections with respect to the residual interaction. Near half-filling, the result of the conductance for even N_C shows a valley-like structure in the ϵ_d dependence. Comparing with the Hartree-Fock results, we see that the self-energy corrections make the valley deep and wide. This is consistent with the tendency towards the development of a Mott-Hubbard insulator gap, and we have examined this feature both for one-dimensional chain

and two dimensional lattice. For odd N_C the correlation effects make the conductance peak, which is seen in the ϵ_d dependence near half-filling, flat. This can be regarded as a manifestation of the Kondo effect, and we have carried out the calculations for odd N_C using a one-dimensional chain.

In the finite system connected to reservoirs, the conductance shows a peak when a resonance state pass through the Fermi energy. Especially, away from half-filling the peak structure can be seen by changing the value of ϵ_d . The behavior of the resonance states can also be analyzed in terms of an extended version of a local Fermi-liquid theory. The presence of the noninteracting leads makes it possible to construct an effective Hamiltonian of a bilinear form, which reproduces exactly the conductance and the total charge displacement of the interacting system at $T = 0$. In this paper we demonstrate using the order U^2 self-energy corrections that the eigenvalue of the effective Hamiltonian can be used also away from half-filling for investigating the position of the resonance states.

Horvatić and Zlatić have shown for the single impurity Anderson model that the radius of the convergence of the perturbation expansion with respect to U decreases rapidly when the system goes away from half-filling.²⁵⁾ The same thing happens also for systems consisting of a number of interacting sites, and away from half-filling the second-order perturbation theory is applicable for relatively small values of U compared to that at half-filling. Therefore, in the present work we have concentrated on the weak interaction cases, and have checked the applicability by comparing the occupation number which are obtained with the two different ways; *i*) integration of the density of states up to the Fermi level, and *ii*) the Friedel sum rule. The results obtained with these two methods agree well for small U .

In §2, we describe the model and formulations for studying the correlation effects away from half-filling. In §3, we present the results of the conductance and the average number of electrons, and discuss the interpretation based on the effective Hamiltonian. Summary is given in §4.

2. Model and Formulation for away from Half-filling

In the system without the translational invariance, the spatial distribution of the charge is usually not uniform, except for the electron-hole symmetric case where the average number of electrons on each site is fixed as one. Therefore, away from half-filling, the charge distribution depends on the parameters of the Hamiltonian, and an extra care is necessary to construct the unperturbed part appropriately. In this section, we describe the outline of the approach: the unperturbed part is determined with the Hartree-Fock approximation assuming that the ground state to be paramagnetic, and then the electron correlation is taken into account using the perturbation expansion with respect to the residual interaction.

Fig. 1 shows the schematic picture of the model, where the lattice sites (quantum dots) are labeled with the coordinate $\mathbf{r} = (i, j)$. The interacting region, where the onsite repulsion U is finite,

consists of M rows in the y -direction and N columns in the x -direction: t_x and t_y are the nearest-neighbor hopping matrix elements in the x - and y -directions, respectively. At the columns of $x = 1$ and $x = N$, the interacting region is connected to noninteracting leads with the mixing matrix elements v_L and v_R , which are assumed to be uniform in the y -direction. The total Hamiltonian \mathcal{H} is given by

$$\mathcal{H} \equiv \mathcal{H}^0 + \mathcal{H}_C^{\text{int}}, \quad (1)$$

$$\mathcal{H}^0 \equiv \mathcal{H}_L + \mathcal{H}_R + \mathcal{H}_C^0 + \mathcal{H}_{\text{mix}}, \quad (2)$$

$$\mathcal{H}_L = \sum_{k\sigma} \epsilon_{Lk} a_{Lk\sigma}^\dagger a_{Lk\sigma}, \quad \mathcal{H}_R = \sum_{k\sigma} \epsilon_{Rk} a_{Rk\sigma}^\dagger a_{Rk\sigma}, \quad (3)$$

$$\begin{aligned} \mathcal{H}_C^0 &= \sum_{i=1}^{N-1} \sum_{j=1}^M \sum_{\sigma} \left[-t_x c_{i+1,j,\sigma}^\dagger c_{i,j,\sigma} + \text{H.c.} \right] \\ &+ \sum_{i=1}^N \sum_{j=1}^M \sum_{\sigma} \left[-t_y c_{i,j+1,\sigma}^\dagger c_{i,j,\sigma} + \text{H.c.} \right] \\ &+ \sum_{i=1}^N \sum_{j=1}^M E_{i,j} (n_{i,j,\uparrow} + n_{i,j,\downarrow}), \end{aligned} \quad (4)$$

$$E_{i,j} \equiv \epsilon_d + \frac{\langle n_{i,j} \rangle_0}{2} U, \quad (5)$$

$$\mathcal{H}_C^{\text{int}} = U \sum_{i=1}^N \sum_{j=1}^M \left[n_{i,j,\uparrow} n_{i,j,\downarrow} - \frac{\langle n_{i,j} \rangle_0}{2} (n_{i,j,\uparrow} + n_{i,j,\downarrow}) \right], \quad (6)$$

$$\mathcal{H}_{\text{mix}} = \sum_{j=1}^M \sum_{\sigma} \left[v_L a_{L,j,\sigma}^\dagger c_{1,j,\sigma} + v_R a_{R,j,\sigma}^\dagger c_{N,j,\sigma} + \text{H.c.} \right]. \quad (7)$$

Here $c_{i,j,\sigma}^\dagger$ creates an electron with spin σ at $\mathbf{r} = (i, j)$, and $n_{i,j,\sigma} = c_{i,j,\sigma}^\dagger c_{i,j,\sigma}$. The periodic boundary condition is assumed along the y -direction $c_{i,M+1,\sigma} \equiv c_{i,1,\sigma}$. In eq. (5), ϵ_d is the bare onsite energy, and $\langle n_{i,j} \rangle_0 \equiv \sum_{\sigma} \langle n_{i,j,\sigma} \rangle_0$ is the non-magnetic solution of the Hartree-Fock approximation: $\langle n_{i,j,\uparrow} \rangle_0 = \langle n_{i,j,\downarrow} \rangle_0$, this average generally depends on the position (i, j) . The Hamiltonian for the two leads, \mathcal{H}_L and \mathcal{H}_R , are written in terms of the one-particle energy $\epsilon_{\lambda k}$ and corresponding eigenfunction $\phi_{\lambda k}(\mathbf{r}_\lambda)$ for $\lambda = L, R$. The operator $a_{\lambda,j,\sigma} = \sum_k a_{\lambda k\sigma} \phi_{\lambda k}(\mathbf{r}_{\lambda,j})$ appearing in the mixing Hamiltonian \mathcal{H}_{mix} annihilates an electron at the interface $\mathbf{r}_{\lambda,j}$. We will be using units $\hbar = 1$ unless otherwise noted.

The single-particle Green's function is defined by

$$G_{\mathbf{r}\mathbf{r}'}(i\varepsilon_n) = - \int_0^\beta d\tau \left\langle T_\tau c_{\mathbf{r}\sigma}(\tau) c_{\mathbf{r}'\sigma}^\dagger(0) \right\rangle e^{i\varepsilon_n \tau}. \quad (8)$$

Here $\beta = 1/T$, $\varepsilon_n = (2n + 1)\pi/\beta$, $c_{\mathbf{r}\sigma}(\tau) = e^{\tau\mathcal{H}} c_{\mathbf{r}\sigma} e^{-\tau\mathcal{H}}$ with $\mathbf{r} = (i, j)$, and $\langle \dots \rangle$ denotes the thermal average $\text{Tr} [e^{-\beta\mathcal{H}} \dots] / \text{Tr} e^{-\beta\mathcal{H}}$. Since U is acting only in the central region (C), the Dyson

equation can be written as

$$G_{\mathbf{r}\mathbf{r}'}(i\varepsilon_n) = G_{\mathbf{r}\mathbf{r}'}^0(i\varepsilon_n) + \sum_{\mathbf{r}_1, \mathbf{r}_2 \in \mathcal{C}} G_{\mathbf{r}\mathbf{r}_1}^0(i\varepsilon_n) \Sigma_{\mathbf{r}_1\mathbf{r}_2}(i\varepsilon_n) G_{\mathbf{r}_2\mathbf{r}'}(i\varepsilon_n). \quad (9)$$

Here $G_{\mathbf{r}\mathbf{r}'}^0(i\varepsilon_n)$ is the unperturbed Green's function corresponding to \mathcal{H}^0 , which is determined with the non-magnetic solution of the Hartree-Fock approximation, so that

$$\langle n_{\mathbf{r}} \rangle_0 = -\frac{2}{\pi} \int_{-\infty}^0 d\omega \operatorname{Im} G_{\mathbf{r}\mathbf{r}}^{0+}(\omega). \quad (10)$$

The value of $\langle n_{\mathbf{r}} \rangle_0$ is determined self-consistently from eqs. (5) and (10). To specify the various types of the Green's functions, we use the symbol $+$ ($-$) in the superscript as a label for the retarded (advanced) function, i.e., $G_{\mathbf{r}\mathbf{r}'}^{\pm}(\omega) \equiv G_{\mathbf{r}\mathbf{r}'}(\omega \pm i0^+)$. In eq. (9), $\Sigma_{\mathbf{r}\mathbf{r}'}$ is the self-energy correction beyond the mean-field theory, and the summations with respect to \mathbf{r}_1 and \mathbf{r}_2 run over the $N_{\mathcal{C}} = N \times M$ sites in the central region. Therefore, the Dyson equation can be written in a matrix form,

$$\{\hat{\mathcal{G}}(z)\}^{-1} = \{\hat{\mathcal{G}}^0(z)\}^{-1} - \hat{\Sigma}(z), \quad (11)$$

$$\{\hat{\mathcal{G}}^0(z)\}^{-1} = z\hat{\mathbf{1}} - \hat{\mathcal{H}}_{\mathcal{C}}^0 - \hat{\mathcal{V}}_{\text{mix}}(z). \quad (12)$$

Here $\hat{\mathcal{G}}^0(z)$ is the $N_{\mathcal{C}} \times N_{\mathcal{C}}$ matrix corresponding to the unperturbed Green's function $G_{\mathbf{r}\mathbf{r}'}^{0+}(\omega)$, $\hat{\mathbf{1}}$ is the $N_{\mathcal{C}} \times N_{\mathcal{C}}$ unit matrix, and

$$\hat{\mathcal{H}}_{\mathcal{C}}^0 = \begin{bmatrix} \mathbf{h}_1^0 & -t_x \mathbf{1} & & \mathbf{0} \\ -t_x \mathbf{1} & \mathbf{h}_2^0 & \ddots & \\ & \ddots & \ddots & -t_x \mathbf{1} \\ \mathbf{0} & & -t_x \mathbf{1} & \mathbf{h}_N^0 \end{bmatrix}, \quad (13)$$

$$\hat{\mathcal{V}}_{\text{mix}}(z) = \begin{bmatrix} v_{\text{L}}^2 \mathbf{F}_{\text{L}}(z) & & & \\ & \mathbf{0} & & \\ & & & v_{\text{R}}^2 \mathbf{F}_{\text{R}}(z) \end{bmatrix}, \quad (14)$$

$$\hat{\Sigma}(z) = \begin{bmatrix} \Sigma_{11}(z) & \Sigma_{12}(z) & \dots & \Sigma_{1N}(z) \\ \Sigma_{21}(z) & \Sigma_{22}(z) & \ddots & \vdots \\ \vdots & \ddots & \ddots & \vdots \\ \Sigma_{N1}(z) & \dots & \dots & \Sigma_{NN}(z) \end{bmatrix}. \quad (15)$$

In eq. (13), $\mathbf{1}$ is the $M \times M$ unit matrix, and \mathbf{h}_i^0 is a tridiagonal $M \times M$ matrix consisting of $E_{i,j}$ at the j -th main diagonal part and $-t_y$ at sub- and superdiagonal parts. In eq. (15), $\Sigma_{ii'}(z)$ is a

$M \times M$ matrix whose (j, j') element is the self-energy $\Sigma_{\mathbf{r}\mathbf{r}'}$ for $\mathbf{r} = (i, j)$, $\mathbf{r}' = (i', j')$. In eq. (14), $\mathbf{F}_\lambda(z) = \{F_{\lambda, jj'}(z)\}$ is the Green's function at the interface of the isolated lead at $\lambda = \text{L, R}$;

$$F_{\lambda, jj'}(z) = \sum_k \frac{\phi_{\lambda k}(\mathbf{r}_{\lambda, j}) \phi_{\lambda k}^*(\mathbf{r}_{\lambda, j'})}{z - \epsilon_{\lambda k}}. \quad (16)$$

From this and the hybridization v_λ , the level width due to the mixing with the leads is given by $\mathbf{\Gamma}_\lambda(\omega) \equiv -v_\lambda^2 \text{Im} \mathbf{F}_\lambda^+(\omega)$ for $\lambda = \text{L}$ and R . In the present study, we assume a diagonal form $\mathbf{F}_\text{L}^+(\omega) = \mathbf{F}_\text{R}^+(\omega) = -i\pi\rho \mathbf{1}$ taking the local density of states at the interfaces ρ to be a constant independent of ω , so that the effects of the mixing can be parameterized by $\Gamma_\lambda = \pi\rho v_\lambda^2$. Note that, because of the periodic boundary condition in the y -direction, the $M \times M$ matrix functions can be diagonalized as $\Sigma_{ii'} = \sum_{m=1}^M \chi_m \Sigma_{ii'}^{(m)} \chi_m^\dagger$. Here χ_m is the eigenvector for the subbands, and the corresponding eigenvalue is given by $\epsilon_m = -2t_y \cos(2\pi m/M)$ for $m = 1, 2, \dots, M$.

At zero temperature, the dc conductance can be calculated from the Green's function as

$$g = \frac{2e^2}{h} \text{Tr} [4\mathbf{\Gamma}_\text{R}(0) \mathbf{G}_{N1}^+(0) \mathbf{\Gamma}_\text{L}(0) \mathbf{G}_{1N}^-(0)], \quad (17)$$

where $\mathbf{G}_{ii'}(z)$ is a $M \times M$ matrix that corresponds to the (i, i') partitioned part of $\widehat{\mathcal{G}}(z)$. Furthermore, at $T = 0$, the total charge displacement ΔN_{tot} can be calculated from the Friedel sum rule,^{22,28)} as

$$\Delta N_{\text{tot}} = \frac{1}{\pi i} \log[\det \mathbf{S}], \quad (18)$$

$$\mathbf{S} = \begin{bmatrix} \mathbf{1} & \mathbf{0} \\ \mathbf{0} & \mathbf{1} \end{bmatrix} - 2i \begin{bmatrix} \mathbf{\Gamma}_\text{L}(0) & \mathbf{0} \\ \mathbf{0} & \mathbf{\Gamma}_\text{R}(0) \end{bmatrix} \begin{bmatrix} \mathbf{G}_{11}^+(0) & \mathbf{G}_{1N}^+(0) \\ \mathbf{G}_{N1}^+(0) & \mathbf{G}_{NN}^+(0) \end{bmatrix}. \quad (19)$$

Specifically, in the case of the constant density of states ρ , the Anderson compensation theorem holds,²⁹⁾ and then the charge displacement of whole the system coincides with the number of electrons in the central region:²²⁾

$$\Delta N_{\text{tot}} = \sum_{i=1}^N \sum_{j=1}^M \langle n_{i,j} \rangle. \quad (20)$$

These expressions, eqs. (17) and (18), show that at $T = 0$ the conductance and charge displacement can be determined by the value of the Green's function at the Fermi energy $\omega = 0$. Therefore, one can introduce a noninteracting Hamiltonian that leads exactly the same g and ΔN_{tot} of the interacting system.²³⁾ This is due to the property $\text{Im} \widehat{\Sigma}^+(0) = \widehat{\mathbf{0}}$ at $T = 0$, and in the central region such an effective Hamiltonian can be constructed as

$$\widehat{\mathcal{H}}_\text{C}^{\text{eff}} = \widehat{\mathcal{H}}_\text{C}^0 + \text{Re} \widehat{\Sigma}^+(0). \quad (21)$$

Note that the self-energy is defined with respect to the whole system, so that $\text{Re } \widehat{\Sigma}^+(0)$ depends not only on U but also on Γ_L and Γ_R through the unperturbed Green's function $\widehat{\mathcal{G}}^0(z)$. We see in the next section that the eigenvalues of $\widehat{\mathcal{H}}_C^{\text{eff}}$ correspond approximately to the peaks of the resonant states.

3. the Second Order Perturbation Theory

In this section, we calculate the self-energy $\text{Re } \widehat{\Sigma}^+(0)$ up to the second order with respect to $\mathcal{H}_C^{\text{int}}$ defined by eq. (6), and show the results for the conductance and charge displacement. In order to determine the unperturbed Green's function $G_{\mathbf{r}\mathbf{r}'}^0$ with the Hartree-Fock approximation assuming the paramagnetic ground state, we calculate first the value of $E_{i,j}$ by solving eqs. (5) and (10) for given ϵ_d and U . Then, we take into account the lowest order self-energy correction due to the fluctuation $\mathcal{H}_C^{\text{int}}$. It is described by the diagram shown in Fig. 2, and its value at $T = 0$ and $\omega = 0$ is given by

$$\Sigma_{\mathbf{r}\mathbf{r}'}^+(0) = -U^2 \int_{-\infty}^{\infty} \int_{-\infty}^{\infty} \frac{d\varepsilon d\varepsilon'}{(2\pi)^2} G_{\mathbf{r}\mathbf{r}'}^0(i\varepsilon) G_{\mathbf{r}\mathbf{r}'}^0(i\varepsilon') G_{\mathbf{r}'\mathbf{r}}^0(i\varepsilon + i\varepsilon'). \quad (22)$$

The explicit form of $G_{\mathbf{r}\mathbf{r}'}^0$ can be derived from eq. (12). Note that the retarded function at $\omega = 0$ and $T = 0$ can be obtained from the Matsubara function, i.e., $\Sigma_{\mathbf{r}\mathbf{r}'}^+(0) = \Sigma_{\mathbf{r}\mathbf{r}'}^+(i\varepsilon)|_{\varepsilon \rightarrow 0^+}$. From eq. (22), one can also confirm explicitly the property $\text{Im } \Sigma_{\mathbf{r}\mathbf{r}'}^+(0) = 0$, at $\omega = 0$ and $T = 0$. We calculate all the $N_C \times N_C$ elements of $\text{Re } \Sigma_{\mathbf{r}\mathbf{r}'}^+(0)$ carrying out the integrations numerically. Then, we obtain the full Green's function $G_{\mathbf{r}\mathbf{r}'}^+$ substituting $\text{Re } \Sigma_{\mathbf{r}\mathbf{r}'}^+(0)$ into the Dyson equation eq. (11).

In the previous work we have used this method to study the ground state properties at half-filling,²²⁾ where the spatial distribution of the charge is uniform independent of the details of the parameters. In this case the perturbation theory works rather well.²³⁾ Specifically, for the single Anderson impurity model, which corresponds to a special limit $N_C = 1$, the order U^2 self-energy describes the low-energy Fermi-liquid behavior properly¹⁷⁾ and gives the spectral function that is qualitatively correct even for rather large U .¹⁶⁾ Away from half-filling, however, the spatial distribution of the charge is inhomogeneous, and it makes the applicability of the second-order perturbation theory rather worse. As the density functional theory²⁴⁾ teaches us, in order to get the ground state correctly, one needs the method that can reproduce the charge distribution accurately. We know the correct charge distribution at half-filling but we do not away from half-filling. Therefore, away from half-filling the charge distribution is the quantity that should be calculated. This makes the situation away from half-filling different from that at half-filling. For the Anderson impurity, the second-order perturbation theory has been applied to away from half-filling,²⁵⁾ and a modified method has also been examined by several authors.^{26,27)} Horvatić and Zlatić has shown for the Anderson model that the radius of the convergence of the perturbation

expansion with respect to U decreases rapidly when the system goes away from half-filling.²⁵⁾ We see that there is a similar tendency also for $N_C > 1$ in the following subsection. To check the applicability of the approximation, we calculate the total charge in the interacting region with two different methods. The first one is using the integration of the local density of states (DOS) up to the Fermi level,

$$\sum_{i=1}^N \sum_{j=1}^M \langle n_{i,j} \rangle = -\frac{2}{\pi} \int_{-\infty}^0 d\omega \operatorname{Tr} \operatorname{Im} \left[\widehat{\mathcal{G}}^+(\omega) \right] \quad (23)$$

where $\widehat{\mathcal{G}}^+(\omega)$ should be calculated using the order U^2 self energy. The second method is using the Friedel sum rule eqs. (18) and (19), and thus the charge is determined by the value at the Fermi energy $\omega = 0$. The two results agree well for small U , and it gives some insights into the applicability.

In the following subsections, we apply the formulation to the Anderson impurity in §3.1 in order to demonstrate how it works in the simplest case. Then, we examine the one-dimensional chain in §3.2 and the two-dimensional lattice in §3.3. Specifically, we concentrate on the case $\Gamma_L = \Gamma_R$ ($\equiv \Gamma$), where the system has the inversion symmetry.

3.1 Anderson impurity

We consider here the single Anderson impurity that corresponds to the case of $N_C = 1$ ($M = 1$, $N = 1$). In this subsection, we use the width of the resonance peak for the noninteracting case as the unit of the energy, i.e., $\Delta = 2\Gamma$.

In Fig. 3, the average number of electrons at the impurity site $\langle n_d \rangle$ is shown as a function of U for $\epsilon_d/\Delta = -0.3$ and -1.0 . The system has the electron-hole symmetry at the value of U where $\langle n_d \rangle$ is equal to 1.0. For $U/(\pi\Delta) \lesssim 1.0$, the results obtained from the Friedel sum rule (\bullet) agree well with that of the integration of DOS (Δ). The range of U where we have good agreement depends on ϵ_d , but the dependence is weak for small ϵ_d . When the onsite energy ϵ_d is unchanged, the local charge $\langle n_d \rangle$ must be a decreasing function of U and converges to a finite constant in the $U \rightarrow \infty$. Therefore, the upturn seen in Fig. 3 indicates the breakdown of the approximation for large U . In Fig. 3, we have also shown the Hartree-Fock results (dashed lines) for $\epsilon_d/\Delta = -0.3$ and -1.0 . For $U < -2\epsilon_d$ (or equivalently $\langle n_d \rangle > 1.0$), the Hartree-Fock result is larger slightly than that of the second-order perturbation result, although it might be hard to see this feature in the figure. In contrast, for $U > -2\epsilon_d$ (or equivalently $\langle n_d \rangle < 1.0$), the Hartree-Fock results is smaller than that of the perturbation results, and the difference increases with U . These results are consistent with that in the seminal work by Horvatić and Zlatić,²⁵⁾ and suggest that the method is applicable for $U/(\pi\Delta) \lesssim 1.0$.

In Fig. 4, the result of the conductance is shown as a function of $U/(\pi\Delta)$ for several values of $\epsilon_d/\Delta = -0.3, -0.7, -1.0$, and -1.5 . The conductance shows a maximum at half-filling $\langle n_d \rangle = 1$,

which corresponds to $U = -2\epsilon_d$. This is because at half-filling the resonance level is situated exactly at the Fermi level. The change of the position of the resonance state can be traced through the eigenvalue of the effective Hamiltonian $\hat{\mathcal{H}}_C^{\text{eff}}$. For the Anderson model the eigenvalue is given by $\tilde{E}_d \equiv \epsilon_d + U \langle n_d \rangle_0 / 2 + \text{Re} \Sigma^+(0)$, which is plotted as a function of U in Fig. 4 (c). The perfect transmission occurs, when the eigenvalue crosses the Fermi level at $\omega = 0$. In the case of the Anderson impurity, \tilde{E}_d corresponds exactly to the position of the resonance state. However, for larger systems consisting of a number of the interacting sites $N_C > 1$, the precise position of the resonant peaks deviates slightly from the eigenvalue of $\hat{\mathcal{H}}_C^{\text{eff}}$ because of the additional effect of the hybridization $\hat{\mathcal{V}}_{\text{mix}}$ appearing in the right-hand side of eq. (12).

3.2 One-dimensional chain

We next consider one-dimensional chains connected to noninteracting leads, which is the case of $M \equiv 1$ and $N \geq 2$. The system can be regarded as a model for a series of quantum dots or the atomic chain of nanometer size. In the electron-hole symmetric case the second-order perturbation theory described above has already been applied to this model.²³⁾ The results obtained at half-filling show the even-odd oscillatory behavior: the perfect transmission due to resonant tunneling occurs for odd N , while for even N the conductance decreases with increasing N showing a tendency towards the development of a Mott-Hubbard insulator gap. In this subsection, we study the ground state properties away from half-filling. In the following, we use the hopping matrix element t , instead of Δ , as the energy scale, and take the mixing parameter to be $\Gamma/t = 0.75$ in the numerical calculations.

To check the applicability of the perturbation theory in the one-dimensional case, we have compared the number of electrons in the interacting region ΔN_{tot} with the Friedel sum rule and the integration of DOS up to the Fermi level as we have done for the Anderson impurity in the above. Specifically, we have examined the chain of length $N = 3$ and $N = 4$ taking the onsite energy to be $\epsilon_d/t = -0.3$ and -1.0 . Although the results are not shown here, we have obtained the figures, the feature of which is quite similar to that of Fig. 3. The results of the two different methods agree well at $U/(2\pi t) \lesssim 0.7$ both for $N = 3$ and $N = 4$. Therefore, in this subsection we discuss the results obtained in the small U region; $U/(2\pi t) \lesssim 0.7$.

In Figs. 5 and 6, the ground state properties of the chains of length $N = 3$ and $N = 4$ are shown, respectively, where the onsite energy ϵ_d/t is taken to be $(\bullet) -0.3$, $(\circ) -0.7$, and $(\blacktriangle) -1.0$. The system of $N = 3$ and 4 can be regarded as the simplest examples of the odd and even chains, respectively, which capture the essence of the one-dimensional network. Note that the system has the electron-hole symmetry when $U + 2\epsilon_d = 0$. It corresponds to the value of U , at which the local charge becomes $\Delta N_{\text{tot}} = N$ and the conductance shows a maximum (minimum) for odd (even) N . When an eigenvalue in the middle, which is shown in the panel (c) of Figs. 5 and 6, crosses the Fermi

level, the conductance shows a peak. For $N = 3$, this happens only at half-filling in the situations shown in Fig. 5 (c), and the position of the conductance peak coincides exactly with the intersection of the central eigenvalue and the Fermi level. In the case of $N = 4$, the conductance shows some peaks away from half-filling. We see two peaks in the curves for (○) $\epsilon_d/t = -0.7$ and (▲) -1.0 in Fig. 6 (a). These peaks in each of the curves correspond to the eigenvalues which cross the Fermi level at $\omega = 0$ successively in Fig. 6 (c). As mentioned in the above, the position of the resonance peaks deviates from that of the eigenvalue because of the energy-shift due to the hybridization. The conductance for (●) $\epsilon_d/t = -0.3$ in Fig. 6 (c) shows a single peak because only one eigenvalue among the four crosses the Fermi level. In the noninteracting case this feature can be seen also in the ω dependence of the transmission probability, which is shown in Fig. 7 for $\epsilon_d/t = -0.3$. In the solid line (for $N = 4$) two peaks among the four are situated below the Fermi level $\omega = 0$, and they move towards the Fermi level when U is switched on.²¹⁾ These examples show that the eigenvalues contain information about resonant states situated near the Fermi level. We note that away from half-filling not only the off-diagonal part²³⁾ but the diagonal part of $\Sigma_{\mathbf{r}\mathbf{r}'}^+(0)$ is finite and plays an important role on the charge distribution. Furthermore, we note that an analogous description has been used in the translational invariant systems, for which the self-energy can be diagonalized in the \mathbf{k} (wave-vector) space and the dispersion for the quasi-particles has a correction through the \mathbf{k} dependence of the self-energy.

So far, we have discussed mainly the U dependence of the conductance and other quantities. In real quantum dot systems, however, the onsite energy ϵ_d can be controlled by the gate voltage. Therefore, the ϵ_d dependence should also be examined. In Fig. 8 the conductance for (a) $N = 3$ and (b) $N = 4$ is shown as a function of ϵ_d taking the Coulomb interaction to be $U/(2\pi t) = 0.5$. The conductance is symmetric with respect to the half-filled point $\epsilon_d = -U/2$ ($\simeq -1.6t$) because of the electron-hole symmetry of the model. To see the effects of the self-energy correction due to the residual interaction, in the figures we have also shown the Hartree-Fock results (○) obtained using the unperturbed Green's function. In the case of $N = 3$, the conductance shows a peak at half-filling, and the self-energy correction makes it broader. This is due to the Kondo effect, and is consistent with the numerical renormalization group results¹³⁾ for the Anderson impurity. On the other hand, in the case of $N = 4$, the self-energy correction makes the valley of the conductance around the half-filling deep and wide. This can be explained as a tendency towards the development of a Mott-Hubbard insulator gap.

3.3 Two-dimensional lattice

In this subsection we consider the two-dimensional Hubbard model, as a model for a quantum dot superlattice. In the numerical calculations, we take the hopping matrix elements to be isotropic $t_x = t_y$ ($\equiv t$), and take the mixing parameter to be $\Gamma/t = 0.75$. Specifically, we examine a system

of the size $M = 4$, $N = 8$: the number of the interacting sites is $N_C = 4 \times 8$.

In Fig. 9, the conductance and the number of electrons in the interacting region are shown for several values of $\epsilon_d/t = -0.3, -0.7, \text{ and } -1.0$. In the lower panel (b) we see that the local charge ΔN_{tot} , which is obtained using the Friedel sum rule, behaves properly as a decreasing function of U at $U/(2\pi t) \lesssim 0.9$. In this range of U , the results obtained with the integration of the DOS (not shown) agrees with the ones in the panel (b), and we can conclude that the second-order perturbation theory is applicable. The conductance shows the peak when a resonance peak passes through the Fermi level, and shows a minimum at half-filling, i.e., at $U = -2\epsilon_d$ or $\Delta N_{\text{tot}} = 32$. Due to the periodic boundary condition in the y -direction, we can see the contribution of each subband separately. In the case of $M = 4$, the subband energy $\epsilon_m = -2t_y \cos(2\pi m/M)$ is given by $\epsilon_{\text{I}} = 2t_y$, $\epsilon_{\text{II}} = \epsilon_{\text{III}} = 0$, and $\epsilon_{\text{IV}} = -2t_y$, where the labels are assigned as I ($m = 2$), II ($m = 1$), III ($m = -1$), and IV ($m = 0$). In Fig. 10 the results of the conductance are shown separately, where ϵ_d/t is taken to be (a) -0.3 , (b) -0.7 , and (c) -1.0 . The resonance states belonging to the mode I (\bullet) and mode IV (\triangle) are sharp, while the peaks in the curve for the mode II and III (\circ) are broad. Note that the two degenerate subbands, II and III, make the same contribution. Comparing the panels (a)–(c), we see that the number of peaks increases when the onsite energy ϵ_d moves deep inside the Fermi level. This is because the resonant states below the Fermi level can cross the Fermi level when the repulsive interaction U increases. In Fig. 11, the local charge is plotted separately for each subband, where ϵ_d/t is taken to be (\bullet) -0.3 , (\circ) -0.7 , and (\triangle) -1.0 . Naturally, the number of electrons in the subbands at low (high) energies is large (small). A step-like behavior is seen for the mode I and IV. This is because the occupation of the sharp resonance state changes rapidly from 2 to 0, when it crosses the Fermi level.

The feature of the resonance peaks can be compared with the transmission probability in the noninteracting case $U = 0$ which is shown in Fig. 12 for $\epsilon_d/t = -0.3$. In this figure, only the contribution of the mode I (solid line) and mode IV (dashed line) is plotted. The contribution of the mode II and III, which is not shown in Fig. 12, is identical to the dashed line in Fig. 7 because of $\epsilon_{\text{II}} = \epsilon_{\text{III}} = 0$. The sharp peaks seen in the curves for the mode I and IV in Fig. 10 correspond to the ones at the band edge of the noninteracting subband-spectrum. Furthermore, the broad peaks seen in Fig. 10 for the mode II and III correspond to the ones in the middle of the noninteracting subband-spectrum. Therefore, when the interaction is switched on, the resonance peaks which already exist in the noninteracting system still remain changing their position and shape gradually. As discussed in the previous subsections, the eigenvalue of the effective Hamiltonian $\hat{\mathcal{H}}_C^{\text{eff}}$ defined by eq. (21) has an additional information about the position of the resonance peaks. In Fig. 13, the U dependence of the eigenvalues is shown for $\epsilon_d/t = -1.0$. Among $N (= 8)$ eigenvalues in each of the modes, those staying near the Fermi level contribute to the conductance. Comparing with the conductance shown in Fig. 10 (c), the resonant peaks seen in the contribution of the mode I

(IV) corresponds to the lowest (highest) two eigenvalues which cross the Fermi level in Fig. 13 (a). Also, the broad peaks seen in the contribution of the mode II and III in Fig. 10 (c) correspond to the three intersections at Fermi level in Fig. 13 (b). Therefore, from the eigenvalue just below the Fermi level, one can anticipate when the next peak will contribute to the tunneling current. This would not be possible if one sees only the conductance.

In Fig. 14 the conductance of the same two-dimensional lattice is shown as a function of the onsite energy ϵ_d taking the Coulomb interaction to be $U/(2\pi t) = 0.5$. Note that, as mentioned in the previous subsection, ϵ_d can be controlled by the gate voltage. As seen in the lower panel (b), the contributions of the mode I and IV are symmetric with respect to the point $\epsilon_d = -U/2$ ($\simeq -1.6t$) which corresponds to the half-filling. Around this point an *energy gap* of the order of U opens up between these two subbands, which is not present basically in the noninteracting case in Fig. 12. However, since the mode II and III carry the current even in this *energy gap* region, the total conductance is finite in the plotted range of ϵ_d in the upper panel (a). For comparison, the Hartree-Fock result of the total conductance is also shown (dashed line) in Fig. 14 (a). Due to the self-energy correction beyond the Hartree-Fock approximation, the valley of the total conductance around the half-filling becomes deep and wide. Comparing with the one-dimensional chain of $N = 1 \times 4$ [see Fig. 8 (b)], this tendency towards the development of a Mott-Hubbard insulator gap becomes clear in the two-dimensional lattice of $N_C = 4 \times 8$.

4. Summary

In summary, we have studied the effects of electron correlation on the transport through a two-dimensional Hubbard model of finite size connected to two noninteracting leads, as a model for a quantum dot superlattice or materials on a nanometer scale. Specifically, we have examined the ground-state properties away from half-filling by extending the previous work done at half-filling. In the calculations, we determine first the unperturbed Green's function using the non-magnetic solution of the Hartree-Fock approximation, and then take into account the second-order self-energy corrections with respect to the residual interaction that is not included in the mean field approximation. This method works well for small U . However, as it is known for the single Anderson impurity, the radius of the convergence of the expansion with respect to U decreases rapidly when the system goes away half-filling.²⁵⁾ We have checked carefully the applicability of the method through the U dependence of the local charge in the interacting region ΔN_{tot} , and study the transport property at small U where ΔN_{tot} behaves properly as a decreasing function of U .

We have calculated the zero-temperature conductance through the one- and two-dimensional Hubbard systems consisting of several tens of interacting sites. The conductance shows peaks caused by the resonant tunneling as a function of the onsite energy ϵ_d which can be controlled by

the gate voltage, and as a function of the Coulomb interaction U . Our numerical results show that the resonant peaks seen in the conductance have direct correspondence to the eigenvalues of the effective Hamiltonian which describes the quasi-particles of the local Fermi liquid. Furthermore, from the eigenvalue we can get information about the resonance states inside the Fermi level.

The formulation used in the present study can be applied to various systems. We have also been studying how the randomness in the sample affects the transport through small interacting systems: real artificially systems seem more or less to be disordered. We have reported preliminary results obtained at half-filling,³⁰⁾ and we are going to study the effects of the randomness away from half-filling.

Acknowledgements

We would like to thank H. Ishii for valuable discussions. Numerical computation was partly performed at computation center of Nagoya University and at Yukawa Institute Computer Facility. This work was supported by the Grant-in-Aid for Scientific Research from the Ministry of Education, Science and Culture, Japan.

- 1) T. K. Ng and P. A. Lee: Phys. Rev. Lett. **61** (1988) 1768.
- 2) L. I. Glazman and M. E. Raikh: Pis'ma Zh. Eksp. Teor. Fiz. **47** (1988) 378 [JETP Lett. **47** (1988) 452].
- 3) A. Kawabata: J. Phys. Soc. Jpn. **60** (1991) 3222.
- 4) Y. Meir, N. S. Wingreen and P. A. Lee: Phys. Rev. Lett. **66** (1991) 3048; *ibid.* **70** (1993) 2601.
- 5) S. Hershfield, J. H. Davies and J. W. Wilkins: Phys. Rev. B **46** (1992) 7046.
- 6) D. Goldharber-Gordon, H. Shtrikman, D. Mahalu, D. Abusch-Magder, U. Meirav and M. A. Kastner: Nature **391** (1998) 156.
- 7) S. M. Cronenwett, T. H. Oosterkamp and L. P. Kouwenhoven: Science **281** (1998) 540.
- 8) T. H. Oosterkamp, T. Fujisawa, W. G. van der Wiel, K. Ishibashi, R. V. Hijman, S. Tarucha and L. P. Kouwenhoven: Nature **395** (1998) 873.
- 9) Y. Tokura, D. G. Austing and S. Tarucha: J. Phys. Condens. Matter **11** (1999) 6023.
- 10) K. Shiraishi, H. Tamura and H. Takayanagi: Appl. Phys. Lett. **78** (2001) 3702; H. Tamura, K. Shiraishi, T. Kimura and H. Takayanagi: Phys. Rev. B **65** (2002) 85324.
- 11) T. Kimura, H. Tamura, K. Kuroki, K. Shiraishi, H. Takayanagi and R. Arita: Phys. Rev. B **66** (2002) 132508
- 12) W. Izumida, O. Sakai and Y. Shimizu: J. Phys. Soc. Jpn. **66** (1997) 717; *ibid.* **67** (1998) 2444.
- 13) W. Izumida and O. Sakai: Phys. Rev. B **62** (2000) 10260; W. Izumida, O. Sakai and S. Suzuki: J. Phys. Soc. Jpn. **70** (2001) 1045.
- 14) O. Sakai, S. Suzuki, W. Izumida and A. Oguri: J. Phys. Soc. Jpn. **68** (1999) 1640.
- 15) A. Oguri: Phys. Rev. B **56** (1997) 13422 [Errata: **58** (1998) 1690].
- 16) A. C. Hewson: *The Kondo Problem to Heavy Fermions* (Cambridge University Press, Cambridge, 1993).
- 17) K. Yamada: Prog. Theor. Phys. **53** (1975) 970; Prog. Theor. Phys. **54** (1975) 316; K. Yosida and K. Yamada: Prog. Theor. Phys. **53** (1975) 1286.
- 18) V. Zlatić and B. Horvatić: Phys. Rev. B **28** (1983) 6904.
- 19) A. Oguri: Phys. Rev. B **64** (2001) 153305; J. Phys. Soc. Jpn. **71** (2002) 2969.
- 20) G. M. Éliashberg: Zh. Eksp. Teor. Fiz. **41** (1961) 1241 [JETP **14** (1962) 886].
- 21) A. Oguri: J. Phys. Soc. Jpn. **70** (2001) 2666.
- 22) Y. Tanaka, A. Oguri and H. Ishii: J. Phys. Soc. Jpn. **71** (2002) 211.
- 23) A. Oguri: Phys. Rev. B **59** (1999) 12240; Phys. Rev. B **63** (2001) 115305 [Errata: **63** (2001) 249901].
- 24) P. Hohenberg and W. Kohn: Phys. Rev. **136** (1964) B864.
- 25) B. Horvatić and V. Zlatić: Phys. Status Solidi B **99** (1980) 251.
- 26) A. Levy Yeyati, A. Martín and F. Flores: Phys. Rev. Lett. **71** (1993) 2991.

- 27) O. Takagi and T. Saso: J. Phys. Soc. Jpn. **68** (1999) 1997.
- 28) J. S. Langer and V. Ambegaokar: Phys. Rev. **121** (1961) 1090.
- 29) P. W. Anderson: Phys. Rev. **124** (1961) 41.
- 30) Y. Tanaka and A. Oguri: Physica E **18** (2003) 300.

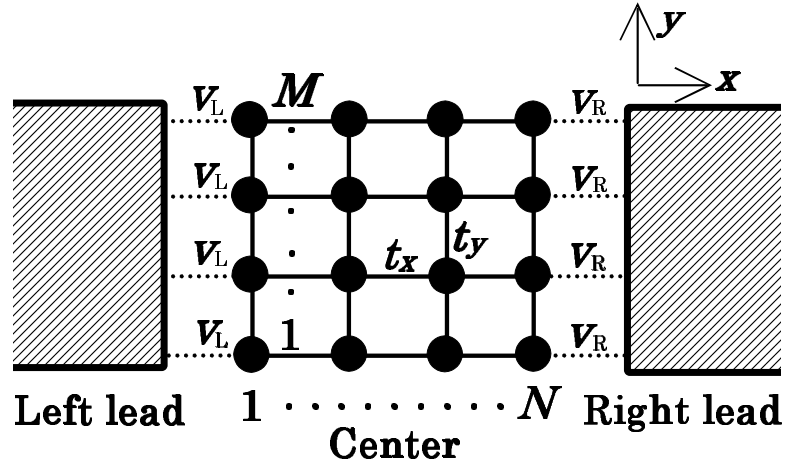


Fig. 1. Schematic picture of the model: (•) interacting sites.

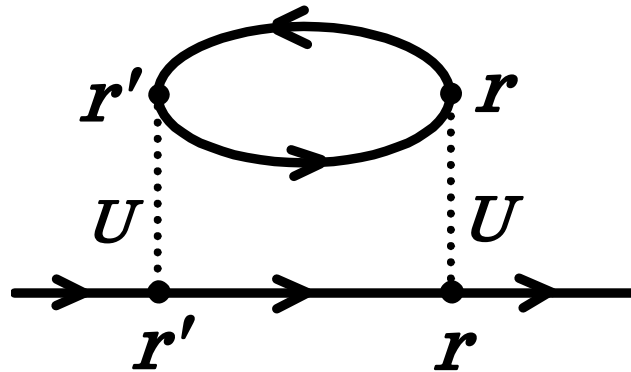


Fig. 2. The order U^2 self-energy $\Sigma_{rr'}(i\varepsilon)$.

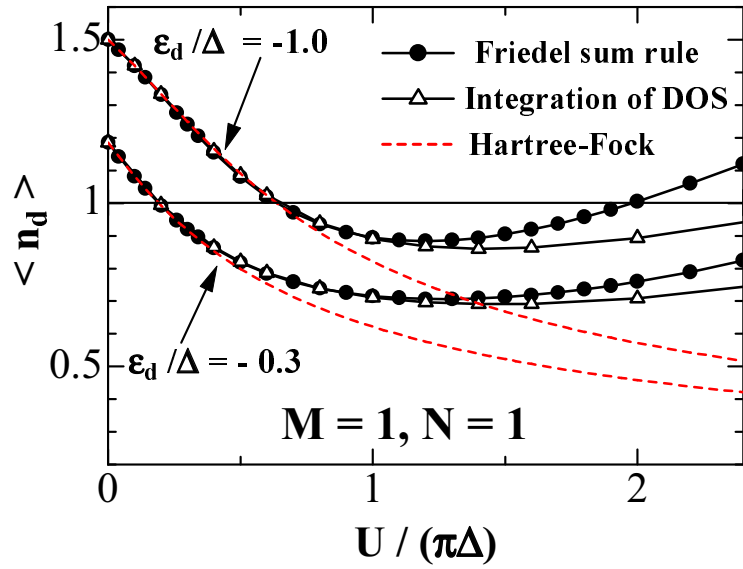


Fig. 3. The number of electrons at the impurity site $\langle n_d \rangle$ of the Anderson model ($M = 1, N = 1$), where ϵ_d/Δ is taken to be -0.3 and -1.0 . The results are obtained with the two different methods which use (\bullet) the Friedel sum rule and (Δ) the integration of DOS up to the Fermi level. The two dashed lines are the results obtained with the Hartree-Fock approximation for the same parameters: $\epsilon_d/\Delta = -0.3$ and -1.0 .

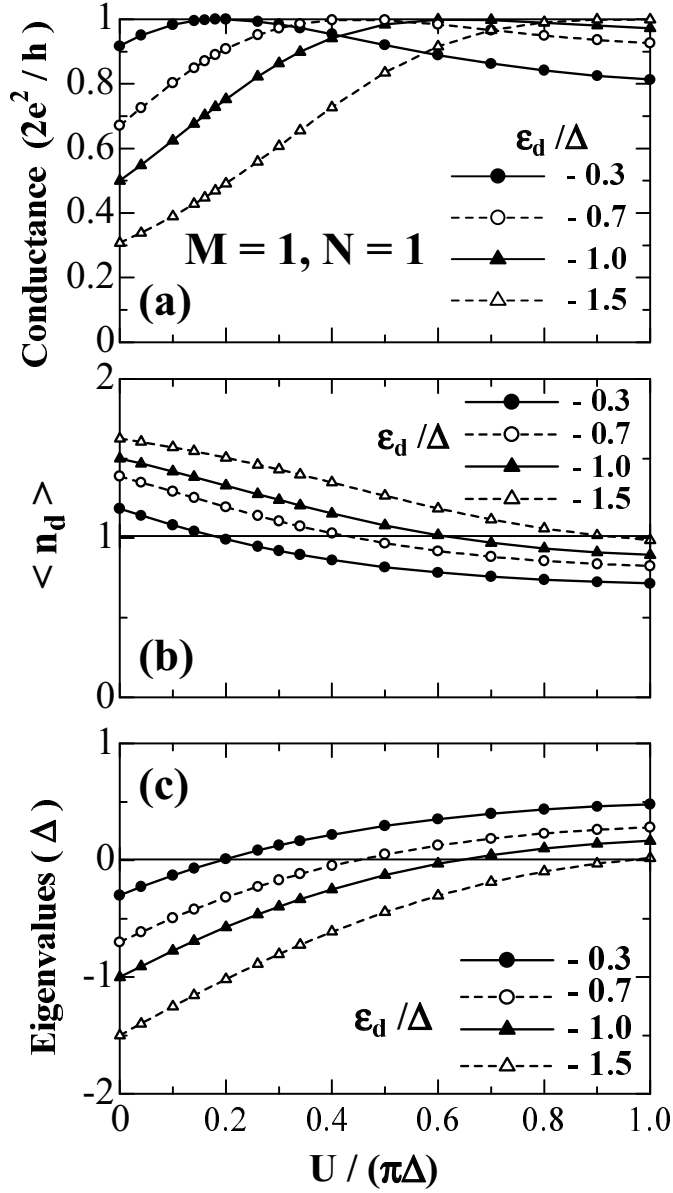


Fig. 4. Ground state properties of the single Anderson model: (a) conductance, (b) local charge $\langle n_d \rangle$, and (c) $\tilde{E}_d \equiv \epsilon_d + U \langle n_d \rangle_0 / 2 + \text{Re} \Sigma^+(0)$ which corresponds to the eigenvalue of $\hat{\mathcal{H}}_C^{\text{eff}}$. Here the onsite energy ϵ_d / Δ is taken to be (●) -0.3, (○) -0.7, (▲) -1.0, and (△) -1.5.

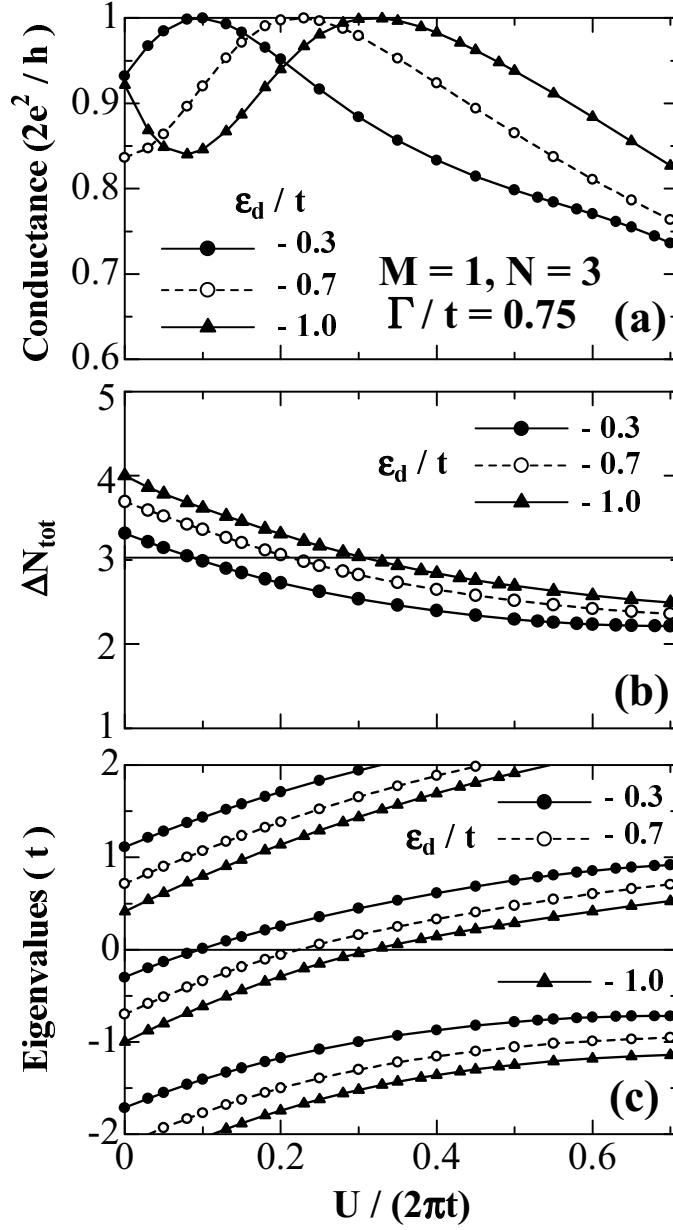


Fig. 5. Ground state properties of a one-dimensional Hubbard model of odd number sites ($M = 1, N = 3$): (a) conductance, (b) local charge in the interacting region $\sum_{i=1}^N \sum_{j=1}^M \langle n_{i,j} \rangle$, and (c) eigenvalues of $\hat{\mathcal{H}}_C^{\text{eff}}$. Here ϵ_d/t is taken to be (●) -0.3 , (○) -0.7 , and (▲) -1.0 .

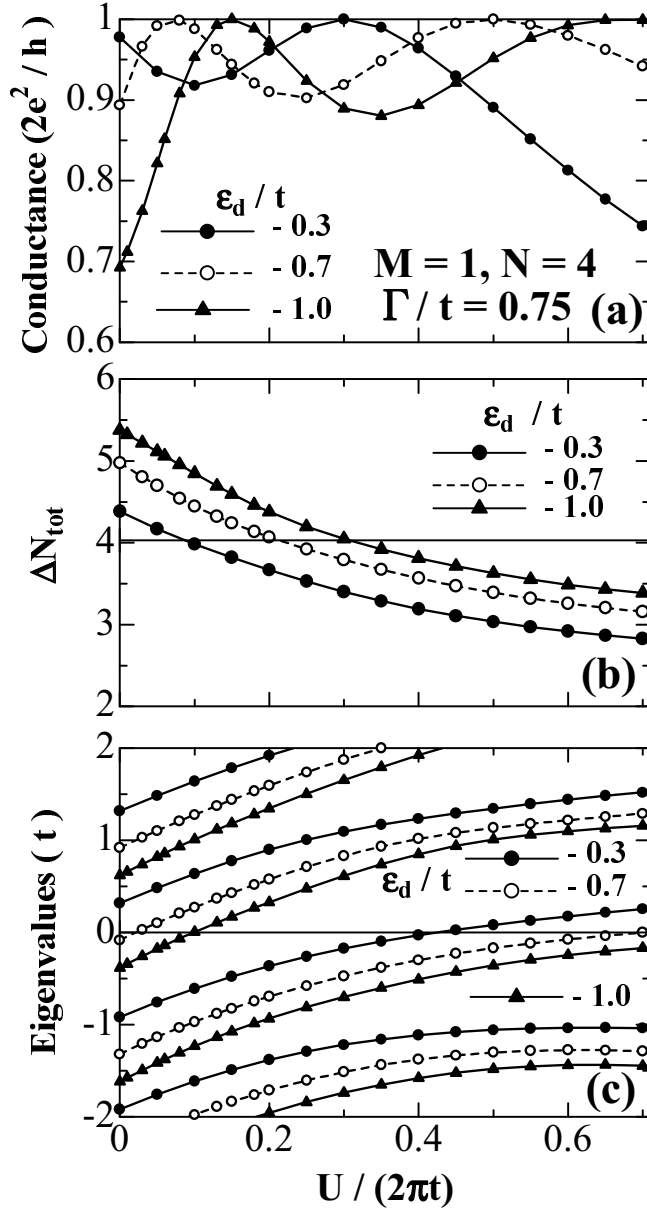


Fig. 6. Ground state properties of a one-dimensional Hubbard model of even number sites ($M = 1, N = 4$): (a) conductance, (b) local charge in the interacting region $\sum_{i=1}^N \sum_{j=1}^M \langle n_{i,j} \rangle$, and (c) eigenvalues of $\hat{\mathcal{H}}_C^{\text{eff}}$. Here ϵ_d/t is taken to be (\bullet) -0.3 , (\circ) -0.7 , and (\blacktriangle) -1.0 .

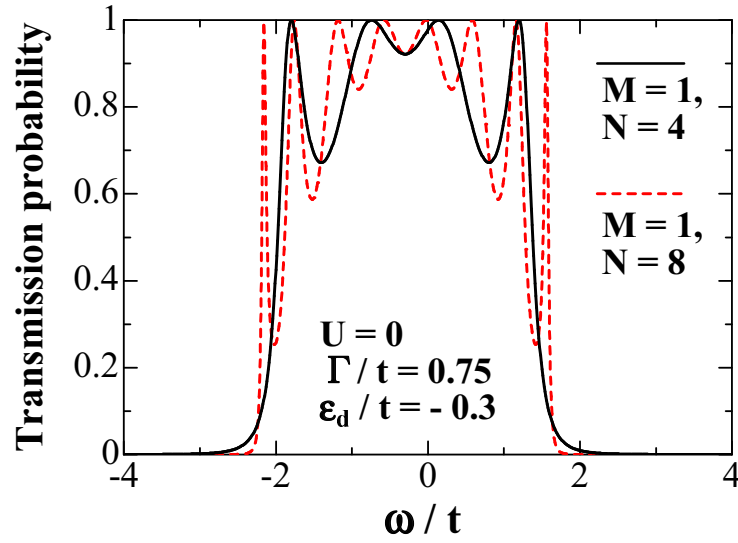


Fig. 7. Transmission probability vs ω for noninteracting chains ($M = 1$), where $\epsilon_d/t = -0.3$ and $\Gamma/t = 0.75$. The solid line is for the system of length $N = 4$, and the dashed line is for $N = 8$.

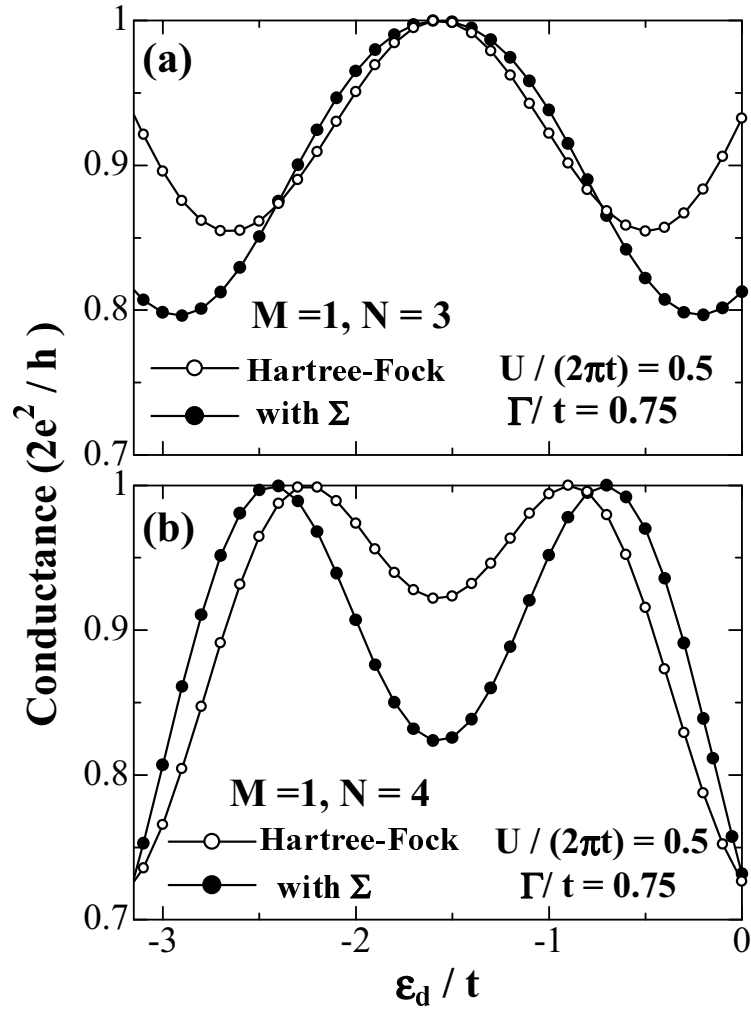


Fig. 8. The ϵ_d dependence of the conductance through the one-dimensional chains ($M=1$) of length (a) $N=3$, and (b) $N=4$. The solid circles (\bullet) denote the results obtained using the second-order self-energy corrections, and the open circles (\circ) denotes the Hartree-Fock results. The Coulomb interaction is taken to be $U/(2\pi t) = 0.5$, so that the electron-hole symmetry holds at $\epsilon_d = -U/2 (\simeq -1.6t)$.

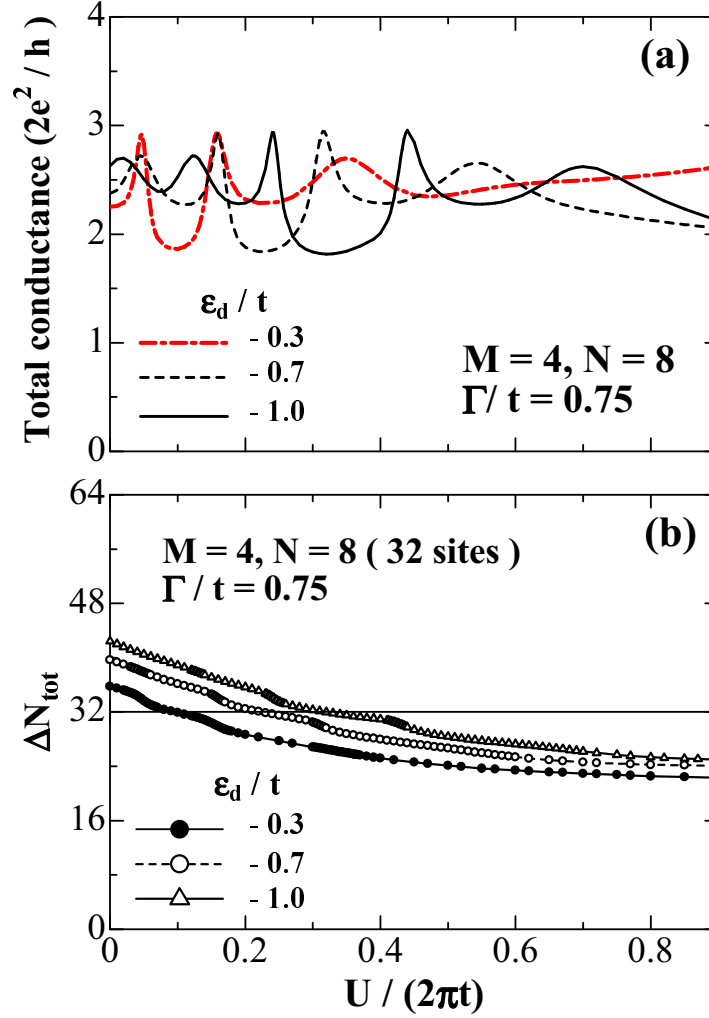


Fig. 9. Ground state properties of the two-dimensional Hubbard model of the size $M = 4$, $N = 8$, (a) total conductance, and (b) local charge in the interacting region $\sum_{i=1}^N \sum_{j=1}^M \langle n_{i,j} \rangle$. Here ϵ_d/t is taken to be (●) -0.3 , (○) -0.7 , and (▲) -1.0 .

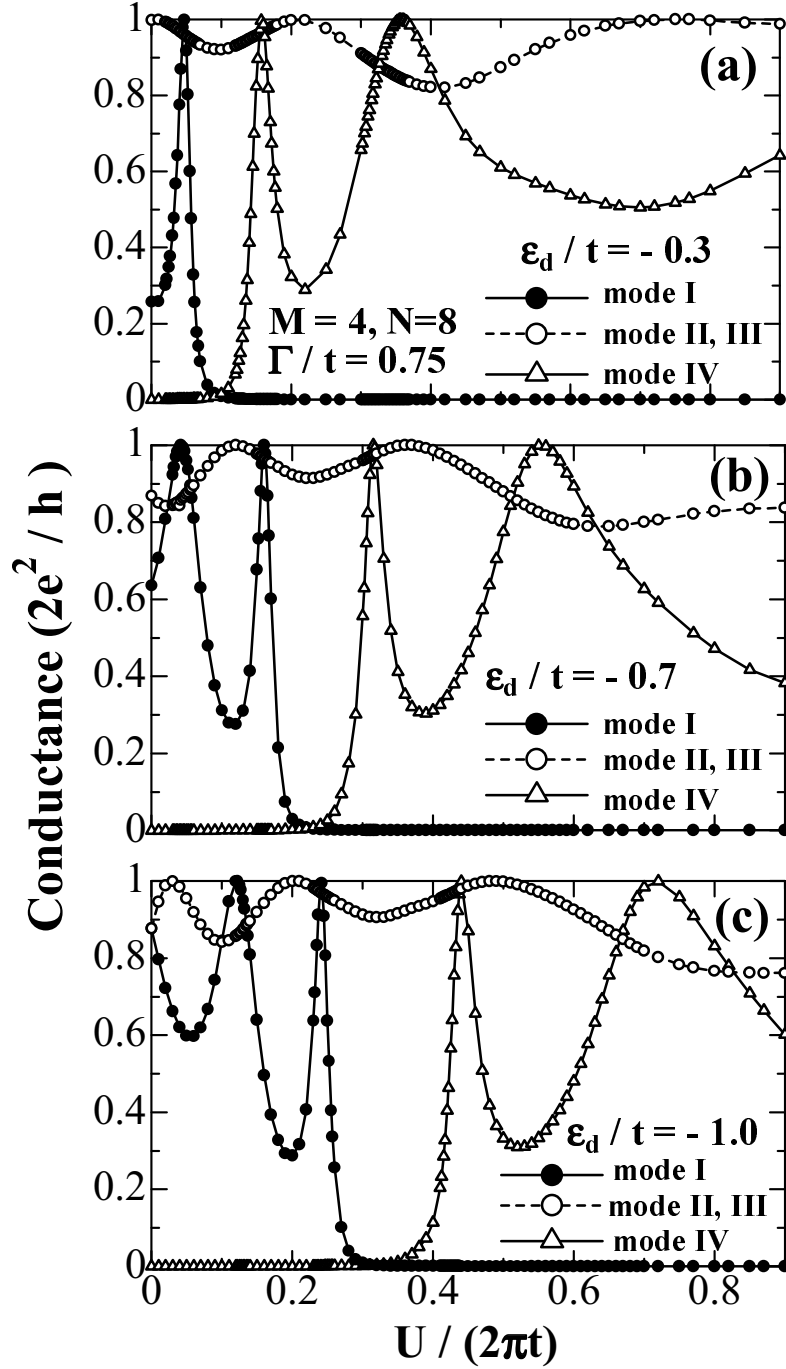


Fig. 10. Contributions of each subband on the conductance of the two-dimensional cluster of the size ($M = 4$, $N = 8$). Here, ϵ_d/t is taken to be (a) -0.3 , (b) -0.7 , and (c) -1.0 .

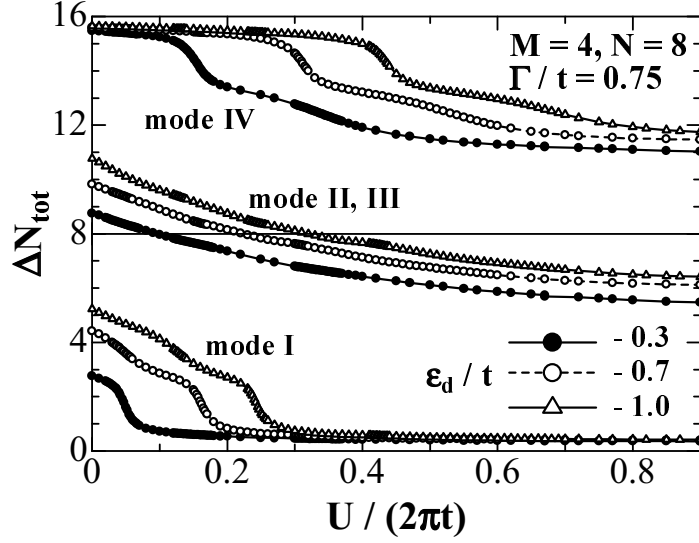


Fig. 11. Contributions of each subband on the local charge in the interacting region $\sum_{i=1}^N \sum_{j=1}^M \langle n_{i,j} \rangle$, of the two-dimensional cluster of the size ($M = 4, N = 8$). Here, ϵ_d/t is taken to be (●) -0.3 , (○) -0.7 , and (△) -1.0 .

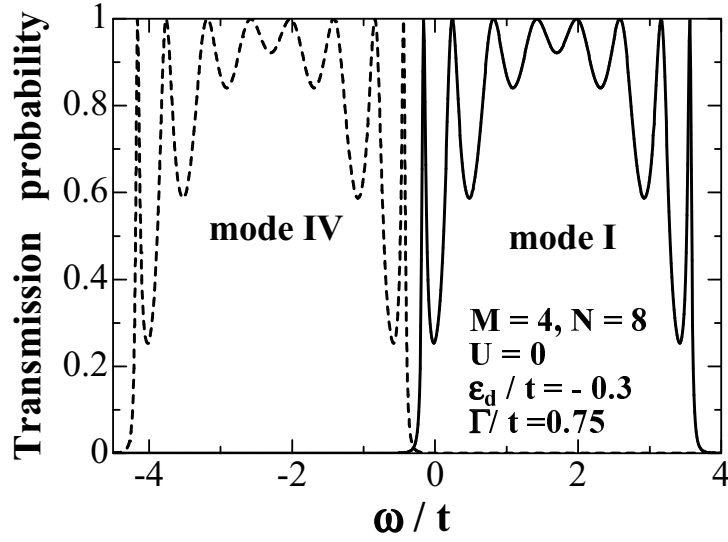


Fig. 12. Transmission probability vs ω for the noninteracting system of the size ($M = 4, N = 8$), for $\epsilon_d/t = -0.3$. Here, only the contribution of the mode I (solid line) and mode IV (dashed line) are plotted. The contribution of the modes II and III corresponds exactly to the dashed line in Fig. 7 that has plotted for a one-dimensional chain.

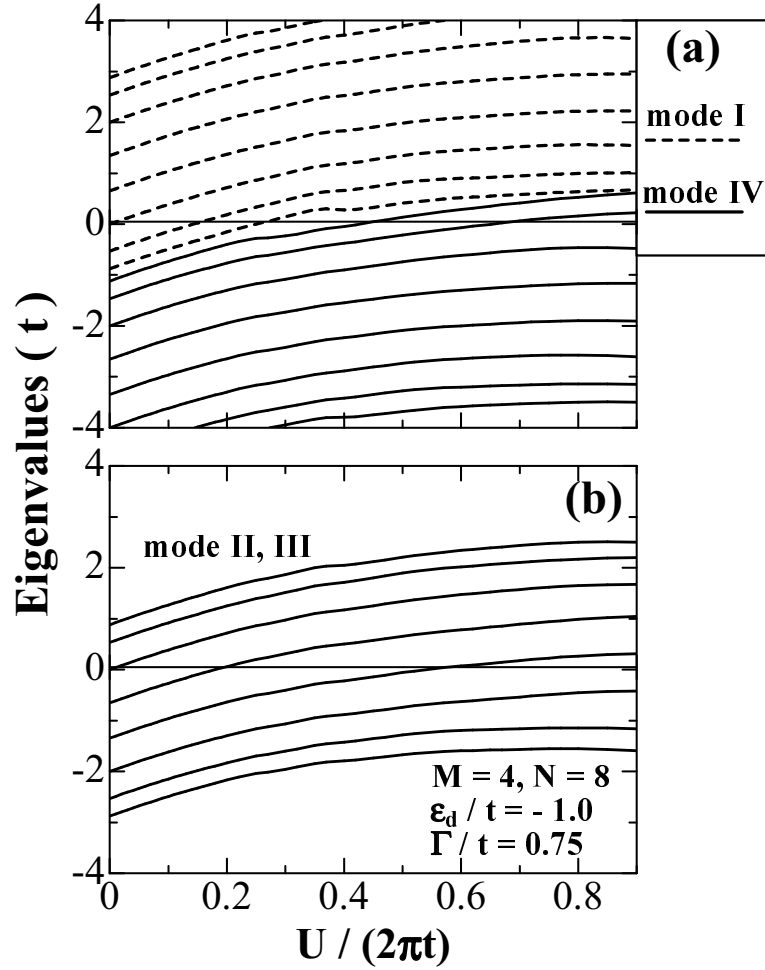


Fig. 13. Eigenvalues of $\hat{\mathcal{H}}_C^{\text{eff}}$ for the two-dimensional Hubbard model of the size ($M = 4, N = 8$). Here, (a) the contribution of the modes I and IV, and (b) that of the degenerate modes II and III. The onsite energy is taken to be $\epsilon_d/t = -1.0$.

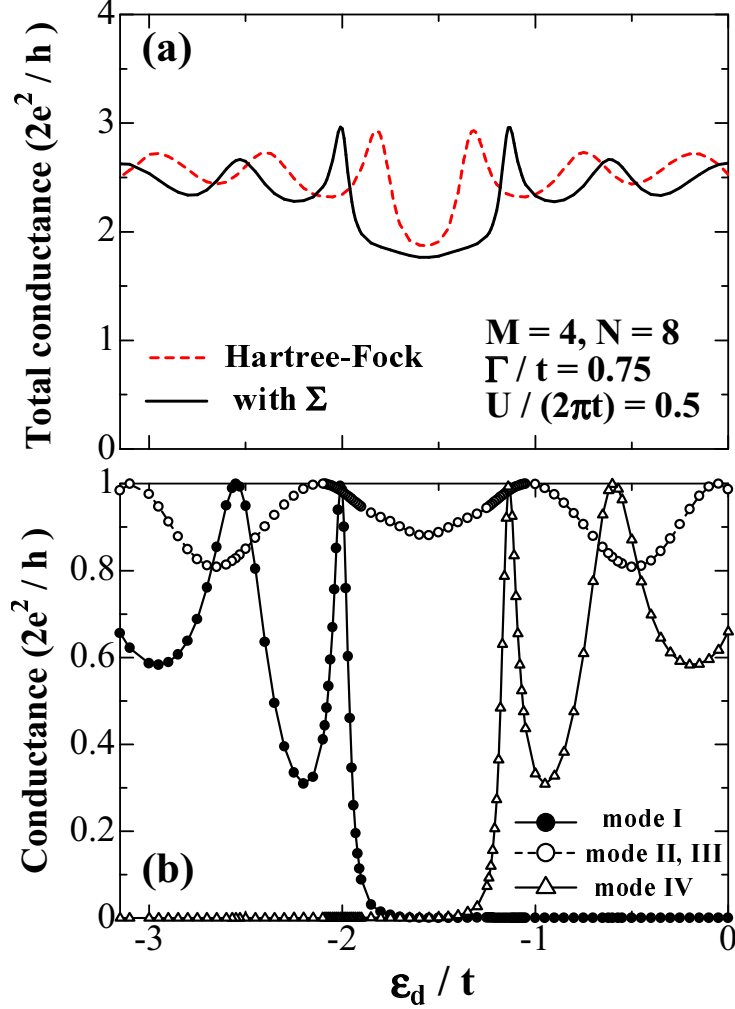


Fig. 14. The ϵ_d dependence of the conductance through the two-dimensional cluster of the size ($M = 4, N = 8$). The upper panel (a) shows the total conductance, where the Hartree-Fock result (dashed line) is also plotted for comparison. The lower panel (b) shows the contribution of each of the modes. The Coulomb interaction is taken to be $U/(2\pi t) = 0.5$, so that the electron-hole symmetry holds at $\epsilon_d = -U/2$ ($\simeq -1.6t$).